Growth kinetics of polymer crystals in bulk

G. Strobl and T.Y. Cho

Physikalisches Institut

Albert-Ludwigs-Universität Freiburg

79104 Freiburg, Germany

Abstract

Temperature dependent measurements of spherulite growth rates carried out for i-polystyrene, poly(ϵ-caprolactone) and linear polyethylene show that the controlling activation barrier diverges at a temperature which is 14K, 22K and 12K, respectively, below the equilibrium melting points. We discuss the existence of such a 'zero growth temperature' T_{zg} in the framework of a recently introduced thermodynamic multiphase scheme and identify T_{zg} with the temperature of a (hidden) transition between the melt and a mesomorphic phase which mediates the crystal growth. The rate determining step in our model of crystal growth is the attachment of chain sequences from the melt onto the lateral face of a mesomorphic layer at the growth front. The necessary straightening of the sequence prior to an attachment is the cause of the activation barrier. A theory based on this view describes correctly the observations. With a knowledge of T_{zg} it is possible to fully establish the nanophase diagram describing the stability ranges of crystalline and mesomorphic layers in a melt. An evaluation of data from small angle X-ray scattering, calorimetry and optical growth rate measurements yields heats of transition and surface free energies of crystals and mesophase layers, as well as the activation barrier per monomer associated with the chain stretching. According to the theory, the temperature dependence of the crystallization rate

is determined by both the activation energy per monomer and the surface free energy of the preceeding mesomorphic layer. Data indicate that the easiness of crystallization in polyethylene is first of all due to a particularly low surface free energy of the mesomorphic layer.

1 Introduction

Different from the large majority of low molar mass systems where crystallization begins immediately when the melt is cooled below the equilibrium melting point, crystallization in polymeric systems is much retarded. A considerable supercooling is necessary before spherulites show up in an optical microscope. At first, they expand slowly so that growth rates can be easily determined. On further cooling the growth rate increases, then passes over a maximum and drops again, down to vanishingly small values when the glass transition is approached. For many crystallizing polymer systems growth rates can be measured through the full temperature range since the maximum values are still low. Polyethylene represents one of the few exceptions. Here growth rates rise to such high values that measurements remain restricted to a certain temperature range below the equilibrium melting point. It is a characteristic property of polymer crystallization that growth rates vary exponentially with temperature, both near the melting point where they decay and near the glass transition where they increase with rising temperature. The behavior indicates control of the growth process by some activation step. Near the glass transition it relates to the diffusive motion of chain sequences which have to pass over intra- and intermolecular activation barriers. Barrier heights are essentially constant so that jump rates increase with rising temperature. The conditions found in the high temperature range near the melting point are different. The slowing down of growth when the temperature goes up is indicative for an increase of the barrier height. In polymers lamellar crystallites form whose thickness also increases when the crystallization temperature is raised. It is an obvious

idea to relate the two observations and to associate the increasing barrier height of the activation step with the increasing thickness of the growing crystallites.

Taking up this idea, Hoffman and Lauritzen [1] developed a model which became popular within short time. Its main assumptions were:

- Crystals grow with a thickness near to their stability limit as given by the Gibbs-Thomson equation, i.e., with a thickness

$$d = \frac{2\sigma_{\mathrm{e}} T_{\mathrm{f}}^{\infty}}{\Delta h_{\mathrm{f}} (T_{\mathrm{f}}^{\infty} - T)} + \delta \tag{1}$$

  where σ_{e} and Δh_{f} denote the surface free energy and the heat of fusion, respectively. According to the equation, crystal thicknesses are inversely proportional to the supercooling below the equilibrium melting temperature T_{f}^{∞} of macroscopic crystals, apart from a minor excess length δ necessary for providing a driving force.

- The activation step is associated with the formation of a secondary nucleus on the growth face. It extends in chain direction over the whole crystallite, i.e., has a length d.

The model treatment yielded an equation for the growth rate u of the form

$$u = u_0 \exp\left(-\frac{T_{\mathrm{A}}}{T - T_{\mathrm{V}}}\right) \exp\left(-\frac{T_{\mathrm{G}}}{T_{\mathrm{f}}^{\infty} - T}\right) \tag{2}$$

The first exponential factor expresses the temperature dependent segmental mobility as given by the Vogel-Fulcher equation (T_{A}: activation temperature, T_{V}: Vogel temperature). The second exponential factor includes the activation energy associated with the formation of a secondary nucleus. This activation energy diverges together with d at T_{f}^{∞}. The Hoffman-Lauritzen model was widely accepted. It became common procedure to evaluate growth rate data of polymer systems as suggested by the theory, and to derive from results surface free energies of the secondary nucleus.

About a decade ago, understanding of polymer crystallization began to change. Eq.(1) was not well founded by experiments. Existing measurements for polyethylene [2] which were taken

as support were not reliable. Polyethylene crystallites thicken in the solid state so that it is very difficult or even impossible to pick up the initial thickness entering into the theory. We therefore carried out time- and temperature dependent small angle X-ray scattering experiments (SAXS) for several other crystallizing polymers which do not have this complication: s- and i-polypropylene, poly(ϵ-caprolactone), poly(1-butene) and octene copolymers of polyethylene [3]; they all keep their crystal thickness constant. The results did not agree with Eq.(1). As it turned out, the law for the temperature dependence of d has also the form of the Gibbs-Thomson equation, however, it includes another controlling temperature, being given by

$$d = \frac{1}{C_{\rm c}(T_{\rm c}^{\infty} - T)} \quad . \tag{3}$$

The temperature $T_{\rm c}^{\infty}$ which determines the crystal thickness is always located above $T_{\rm f}^{\infty}$, in the case of polyethylene about 10K, for poly(ϵ-caprolactone) about 30K and for i-polystyrene about 20K. In addition, it was observed that the thickness of crystals developing at a given temperature does not change if co-units or stereo-defects are incorporated in the chain, whereas the melting points are depressed as expected from Raoult's law.

Eq.(1) turning out to be incorrect, Eq.(2) for the growth rate became doubtful as well. So we performed a check. The first results, obtained for poly(ϵ-caprolactone) (PϵCL)[4] and linear polyethylene (PE) [5], are presented here once again, and they indeed show that Eq.(2) also has to be changed. The measurements show that growth rates are given by an equation with the form of Eq.(2), however, $T_{\rm f}^{\infty}$ has to be replaced by another temperature, the 'zero growth temperature' $T_{\rm zg}$. It is always located below the equilibrium melting point, for PE more than 10K, and in the case of PϵCL even 22K. The correct relationship reads:

$$u = u_0 \exp\left(-\frac{T_{\rm A}}{T - T_{\rm V}}\right) \exp\left(-\frac{T_{\rm G}}{T_{\rm zg} - T}\right) \quad . \tag{4}$$

Hence polymer crystallization and melting are controlled by three characteristic temperatures rather than $T_{\rm f}^{\infty}$ only. Crystallite thicknesses vary with the distance to $T_{\rm c}^{\infty}$, and the growth rate

depends on the distance to T_{zg}. The sequence of the three temperatures is always $T_c^\infty > T_f^\infty > T_{zg}$.

We offered an explanation for the existence of three characteristic temperatures. Since several years we advocate the view that the pathway followed in the growth of polymer crystallites includes an intermediate phase of mesomorphic character[6]. Chain sequences are first attached to the growth front of a mesomorphic layer. The latter thickens spontaneously up to a critical value where block-like crystallites form out of it. Introducing three phases, the scheme includes also three transition temperatures, T_{am}^∞ between the amorphous melt and the mesomorphic phase, T_{mc}^∞ between the mesomorphic phase and the crystallites, and T_{ac}^∞=T_f^∞ for the crystal melting. We identify T_{am}^∞ with T_{zg} and T_{mc}^∞ with T_c^∞.

What is the nature of the activation step? The traditional view - formation of a secondary nucleus - cannot be transferred to the case of a growth face with non-crystalline, mesomorphic structure. In this paper we try to give an answer and present a new approach.

The paper is organized as follows: Section 2 contains a short summary of the 'multi phase scheme' introduced in a general treatment of polymer crystallization and melting [7]. Section 3 presents a new theory for the growth kinetics. Section 4 collects relevant experimental results previously obtained for PϵCL, i-polystyrene (iPS) and PE and additional growth rate data of iPS. The results are commonly discussed in Section 5. The data evaluation yields for the three systems heats of transition and surface free energies of the crystalline and the mesomorphic phase, as well as the activation free energy which controls the growth rate.

2 Thermodynamic scheme treating polymer crystallization and melting

Based on the results of SAXS studies we proposed a pathway of polymer crystallization as it is depicted in the sketch in Fig. 1. A thin layer with mesomorphic inner structure forms between the lateral crystal face and the melt, stabilized by epitaxial forces. Stereo defects and co-units which cannot be incorporated in the mesomorphic phase are rejected at the melt front. A high inner mobility allows a spontaneous thickening of the layer up to a critical value where the core region crystallizes under formation of a block. In a last step the surface region of this block, at first still disordered, perfects, which leads to a further stabilization (see figures 3 and 4 in [8]). The block structure is retained in the final lamella [9].

The thermodynamic conditions under which such a mesomorphic phase can interfere and affect the crystallization process are described in the drawing of Fig. 2. The schematic plot shows for both the crystalline phase (label 'c') and the mesomorphic phase ('m') the difference of the chemical potential to that of the melt ('a'):

$$\begin{aligned} \Delta g_{\mathrm{ac}} &= g_{\mathrm{c}} - g_{\mathrm{a}} \ , \\ \Delta g_{\mathrm{am}} &= g_{\mathrm{m}} - g_{\mathrm{a}} \ . \end{aligned} \tag{5}$$

Coming from high temperatures the chemical potential of the crystalline phase drops below the value of the melt when crossing the equilibrium melting point, here denoted T^{∞}_{ac}. The mesomorphic phase requires a lower temperature, T^{∞}_{am}, to fall with its chemical potential below that of the melt. The plot includes also a temperature T^{∞}_{mc}. It represents the temperature of a hidden transition, namely that between the mesomorphic and the crystalline phase. Since the chemical potential of the crystal is always below that of the mesomorphic phase, the latter is only metastable for macroscopic systems. However, for small objects with sizes in the nm range, stabilities can be inverted. Due to the usually lower surface free energy thin mesomorphic layers

can have a lower Gibbs free energy than a crystallite with the same thickness. As shown by the diagram, the transition temperatures have the order $T_{\rm mc}^{\infty} > T_{\rm ac}^{\infty} > T_{\rm am}^{\infty}$.

Thermodynamics relates the three transition temperatures $T_{\rm am}^{\infty}$, $T_{\rm ac}^{\infty}$, $T_{\rm mc}^{\infty}$ to the entropy increases $\Delta s_{\rm ma} = s_{\rm a} - s_{\rm m}$ and $\Delta s_{\rm ca} = s_{\rm a} - s_{\rm c}$ associates with a melting of the mesomorphic and the crystalline phase, respectively. Since the slopes of $\Delta g_{\rm am}$ and $\Delta g_{\rm ac}$ are given by $\Delta s_{\rm ma}$ and $\Delta s_{\rm ca}$, one can write in linear approximation, neglecting changes of the slopes with temperature,

$$(T_{\rm mc}^{\infty} - T_{\rm ac}^{\infty})\Delta s_{\rm ca} \approx (T_{\rm mc}^{\infty} - T_{\rm am}^{\infty})\Delta s_{\rm ma} \quad , \tag{6}$$

or

$$\frac{\Delta h_{\rm ma}}{\Delta h_{\rm ca}} = \frac{\Delta s_{\rm ma} T_{\rm am}^{\infty}}{\Delta s_{\rm ca} T_{\rm ac}^{\infty}} \approx \frac{(T_{\rm mc}^{\infty} - T_{\rm ac}^{\infty})T_{\rm am}^{\infty}}{(T_{\rm mc}^{\infty} - T_{\rm am}^{\infty})T_{\rm ac}^{\infty}} \quad . \tag{7}$$

The multistage model of Fig.1 can be based on a thermodynamic scheme. It deals with four different phases:

- the amorphous melt
- mesomorphic layers

and two limiting forms of the block-like crystallites, namely

- native crystals (labelled '$\rm c_n$') and
- stabilized crystals (with label '$\rm c_s$').

The scheme, being displayed in Fig. 3, delineates the stability ranges and transition lines for these phases. The variables in this phase diagram are the temperature and the inverse crystal thickness. The thickness is given here by the number n of monomers in a stem, i.e., $n = d/\Delta z$ with Δz denoting the stem length increment per monomer. The transition lines are denoted $T_{\rm mc_n}$ ('crystallization line'), $T_{\rm ac_n}$, $T_{\rm mc_s}$ ('recrystallization line'), $T_{\rm ac_s}$ ('melting line'), $T_{\rm am}$, all to be understood as functions of n^{-1}. They represent equilibria determined by thermodynamics.

$T_{\mathrm{ac_s}}$ is the Gibbs-Thomson line describing crystallite melting already included in Eq.(1) :

$$T_{\mathrm{ac}}^{\infty} - T \approx \frac{2\sigma_{\mathrm{ac_s}}}{\Delta s_{\mathrm{ca}}} \frac{1}{n} = \frac{2\sigma_{\mathrm{ac_s}} T_{\mathrm{ac}}^{\infty}}{\Delta h_{\mathrm{ca}}} \frac{1}{n} \tag{8}$$

(T_{f}^{∞} is renamed in T_{ac}^{∞}, Δh_{ca} is the heat of fusion per monomer, and $\sigma_{\mathrm{ac_s}}$ is the excess free energy of the monomers at surfaces). Proceeding in analogous manner in the derivation of expressions for the other size dependent phase transitions, one obtains for $T_{\mathrm{mc_n}}$ the equation

$$T_{\mathrm{mc}}^{\infty} - T \approx \frac{(2\sigma_{\mathrm{ac_n}} - 2\sigma_{\mathrm{am}})}{\Delta s_{\mathrm{cm}}} \frac{1}{n} \tag{9}$$

and for $T_{\mathrm{mc_s}}$ the equation

$$T_{\mathrm{mc}}^{\infty} - T \approx \frac{(2\sigma_{\mathrm{ac_s}} - 2\sigma_{\mathrm{am}})}{\Delta s_{\mathrm{cm}}} \frac{1}{n} \tag{10}$$

with

$$\Delta s_{\mathrm{cm}} = \Delta s_{\mathrm{ca}} - \Delta s_{\mathrm{ma}} \tag{11}$$

σ_{am} and $\sigma_{\mathrm{ac_n}}$ denote surface free energies. We identify $T_{\mathrm{mc_n}}$ with the experimental relationship Eq.(3) which implies in particular that T_{c}^{∞}, the controlling temperature for the crystal thickness, is set equal to the transition temperature T_{mc}^{∞}. The line T_{am} refers to the transition between the melt and the mesomorphic layer and is correspondingly described by

$$T_{\mathrm{am}}^{\infty} - T \approx \frac{2\sigma_{\mathrm{am}}}{\Delta s_{\mathrm{ma}}} \frac{1}{n} = \frac{2\sigma_{\mathrm{am}} T_{\mathrm{am}}^{\infty}}{\Delta h_{\mathrm{ma}}} \frac{1}{n} \quad . \tag{12}$$

The line begins at the temperature T_{am}^{∞}.

The scheme includes two points, denoted $\mathrm{X_n}$ and $\mathrm{X_s}$, at which three lines cross. The crossing indicates for $\mathrm{X_n}$ the coincidence

$$g_{\mathrm{a}} = g_{\mathrm{m}} + \frac{2\sigma_{\mathrm{am}}}{n} = g_{\mathrm{c}} + \frac{2\sigma_{\mathrm{ac_n}}}{n} \tag{13}$$

and for $\mathrm{X_s}$ the coincidence

$$g_{\mathrm{a}} = g_{\mathrm{m}} + \frac{2\sigma_{\mathrm{am}}}{n} = g_{\mathrm{c}} + \frac{2\sigma_{\mathrm{ac_s}}}{n} \tag{14}$$

$\mathrm{X_n}$ and $\mathrm{X_s}$ thus represent triple points with coinciding Gibbs free energies for amorphous, mesomorphic and crystalline lamellae. The positions of $\mathrm{X_n}$ and $\mathrm{X_s}$ determine what happens during

an isothermal crystallization followed by heating. The scheme predicts two different scenarios; in the figure they are exemplified by the routes A and B, respectively. Route B, realized by crystallizations at high temperatures, is as follows: At the point of entry, labelled '1', chains are attached from the melt onto the front of a mesomorphic layer with minimum thickness. The layer spontaneously thickens until the transition line $T_{\mathrm{mc_n}}$ is reached at point 2, where native crystals form immediately. The subsequently following stabilization transforms them into a lower free energy state. On heating crystallites remain stable up to the transition line $T_{\mathrm{ac_s}}$ associated with a melting of the crystals (point 3). Route A (low crystallization temperatures) is different: The beginning is the same - starting at point 1 with an attachment of chain sequences onto a spontaneously thickening mesomorphic layer, then, on reaching $T_{\mathrm{mc_n}}$, the formation of native crystals (point 2) followed by a stabilization. When heating the stabilized crystals they at first retain their structure. At point 3a the transition line $T_{\mathrm{mc_s}}$ is reached which relates to a transformation into the mesomorphic state instead of melting. The consequence for a further heating is a continuous recrystallization mediated by the mesophase ((3a) to (3b)). This ends at the triple point $\mathrm{X_s}$ (3b) where the crystal melts. Exactly such melting properties with two different scenarios are observed for crystallizing polymers [7][10].

3 Kinetics of lateral growth

If a lamellar crystallite grows following the multistage process from Fig.1, several steps are performed. In the general case, all the steps will equally contribute to the resulting growth rate, but under special circumstances one of the steps can get rate controlling, the other ones becoming adjusted to it. As it appears, this simpler case is found. The observation that the activation barrier diverges at a temperature T_{zg} which can be identified with T_{am}^{∞} indicates that the first step, the attachment of chain sequences to the lateral face of the mesomorphic layer, determines the rate of growth. Starting from this assumption, a kinetical theory can be

formulated in straightforward manner.

Considering about the nature of the activation step, the following idea looks reasonable: Before a sequence, which lies coiled in the melt, is incorporated into the growing mesomorphic layer, it has to be activated by a transfer into the overall straightened form required for an attachment followed by an inclusion - different from the crystal the mesomorphic layer thereby allows for a variety of conformations. The straightening has to reach at least the length set by the initial thickness of the mesomorphic layer given by Eq.(12). The associated conformational free energy, $\Delta F^{\rm con}$, is proportional to the sequence length and changes therefore with temperature according to

$$\Delta F^{\rm con} \propto n \propto \frac{1}{T_{\rm am}^{\infty} - T} \quad . \tag{15}$$

For $T_{\rm zg}$= $T_{\rm am}^{\infty}$ this agrees with the experimental result expressed by Eq.(4), with a barrier height which diverges at $T_{\rm zg}$.

A detailed treatment has to consider the chain dynamics at the growth face of the advancing mesomorphic layer. Growth rates are generally determined by the thermodynamic driving force and the time scale of the processes at the growth front. In order to grow at a given temperature, the mesomorphic layer has to be slightly thicker than the value $n_{\rm eq}$ given by Eq.(12) that separates growing from shrinking layers. We therefore write for the number of monomers in an attached stem

$$n = n_{\rm eq}(T) + \delta n \tag{16}$$

introducing an 'excess length' δn which determines the thermodynamic driving force.

One can directly formulate an expression for the velocity of the growth front, u. At the front there exists a dynamic equilibrium, with sequences of n monomers becoming attached and detached. To describe the resulting growth kinetics we introduce two variables, j_- and j_+, giving the rates of detachment and attachment respectively, taken per single site on the lateral

growth face. u then is given by

$$u = b_{\rm m}(j_+ - j_-) = b_{\rm m} j_+ (1 - \frac{j_-}{j_+}) \tag{17}$$

where $b_{\rm m}$ denotes the monomer diameter. The expression $1 - j_-/j_+$ represents the thermodynamic driving force for a stem of m monomers. It vanishes at equilibrium where attachment and detachment rates are exactly balanced, and increases with the excess length. Near equilibrium, i.e., for a weak driving force, a linear relation holds

$$1 - \frac{j_-}{j_+} = \frac{-\Delta g_{\rm am}}{R T^{\infty}_{\rm am}} \delta n \ . \tag{18}$$

Using

$$-\Delta g_{\rm am} = \Delta s_{\rm ma} (T^{\infty}_{\rm am} - T) \tag{19}$$

the growth rate of a layer with thickness $n_{\rm eq}$ follows as

$$u = b_{\rm m} j_+ \frac{\Delta s_{\rm ma} (T^{\infty}_{\rm am} - T)}{R T^{\infty}_{\rm am}} \delta n \tag{20}$$

For $\delta n > 0$, the case of interest, the attachment rate is larger than the detachment rate and the growth face is shifted towards the melt. Conversely, for $\delta n < 0$, realized if the temperature is increased above the equilibrium melting point of the mesomorphic layer, the detachment rate becomes greater and the growth front moves back. In both cases, the basic time scale is set by the coefficient j_+.

The experimentally observed exponential change of the growth rate with temperature originates from of an exponential dependence of j_+ on the sequence length

$$j_+(n) = j_0 \exp(-\mu n) \tag{21}$$

This is easily seen, by just remembering the kinetical criterion which controls the transformation process: The thickness of the mesomorphic layer growing at a given temperature is that associated with the maximum growth rate. Applying this criterion, we write

$$u(\delta n) \quad = \quad b_{\rm m} j_0 \frac{\Delta s_{\rm ma} (T^{\infty}_{\rm am} - T)}{R T^{\infty}_{\rm am}} \exp(-\mu n) \delta n \tag{22}$$

$$= \quad b_{\mathrm{m}} j_0 \frac{\Delta s_{\mathrm{ma}}(T_{\mathrm{am}}^{\infty} - T)}{R T_{\mathrm{am}}^{\infty}} \exp(-\mu n_{\mathrm{eq}}) \exp(-\mu \delta n) \delta n \tag{23}$$

and search for the maximum. This is located at

$$\delta n = \frac{1}{\mu} \tag{24}$$

and associated with a growth rate

$$u = \frac{b_{\mathrm{m}} j_0 \Delta s_{\mathrm{ma}}(T_{\mathrm{am}}^{\infty} - T)}{\mathrm{e} \mu R T_{\mathrm{am}}^{\infty}} \exp(-\mu n_{\mathrm{eq}}) \tag{25}$$

For j_0 we write, introducing the Vogel-Fulcher relationship,

$$j_0 \propto \exp\left(-\frac{T_{\mathrm{A}}}{T - T_{\mathrm{V}}}\right) \ . \tag{26}$$

As mentioned at the beginning of this section, we propose to associate the activation barrier with the straightening of a chain sequence prior to its attachment, which means to set

$$\mu n = \frac{\Delta F^{\mathrm{con}}}{RT} \ . \tag{27}$$

μ is then identical with the change of the configurational free energy per monomer, denoted Δf^{con}:

$$\mu = \frac{\Delta f^{\mathrm{con}}}{RT} \ . \tag{28}$$

Experiments allow a determination of Δf^{con} based on the following relationships:

- The initial thickness of the mesomorphic layer forming at a temperature T is determined by

$$n_{\mathrm{eq}} = \frac{\Delta h_{\mathrm{ma}}}{2 \sigma_{\mathrm{am}} T_{\mathrm{am}}^{\infty}} \frac{1}{T_{\mathrm{ma}}^{\infty} - T} \tag{29}$$

or

$$d = \Delta z n_{\mathrm{eq}} = \frac{1}{C_{\mathrm{m}}(T_{\mathrm{am}}^{\infty} - T)} \tag{30}$$

- Combination of Eqs.(25),(26),(28) and (30) results in

$$u = u_1 \frac{T_{\mathrm{am}}^{\infty} - T}{T_{\mathrm{am}}^{\infty}} \exp\left(-\frac{T_{\mathrm{A}}}{T - T_{\mathrm{V}}}\right) \exp\left(-\frac{T_{\mathrm{G}}}{T_{\mathrm{am}}^{\infty} - T}\right) \tag{31}$$

with

$$T_{\rm G} = \frac{\Delta f^{\rm con}}{R T_{\rm am}^{\infty} \Delta z C_{\rm m}} \tag{32}$$

As is shown in the following, SAXS, differential scanning calorimetry (DSC) and growth rate measurements yield $C_{\rm m}$ and the 'growth activation temperature' $T_{\rm G}$. The activation barrier per monomer $\Delta f^{\rm con}$ follows from Eq.(32).

4 Experimental results

Growth rate measurements were carried out for PϵCL [4] and linear PE[5], and now additionally for iPS, complementing earlier investigations by SAXS and DSC on the same samples[11][12]. Growth rates of iPS were directly determined in a polarizing optical microscope with a heating stage. The experiment started at 186 °C after a rapid cooling from the melt. Growth of one selected isolated spherulite was observed and registered with a digital camera. Growth rates were measured for this spherulite at a series of temperatures separated by steps of 3 K. Image processing yielded the spherulite area as a function of time, and from the area the radius was derived. The result is presented in Fig.4

Starting off from Eq.(4) it is possible to derive from the data the zero growth temperature $T_{\rm zg}$. We write

$$\ln \frac{u}{u_0} + \frac{T_{\rm A}}{T - T_{\rm V}} = -\frac{T_{\rm G}}{T_{\rm zg} - T} \tag{33}$$

and differentiate. A reordering leads to

$$\left(-\frac{{\rm d} \ln(u/u_0)}{{\rm d}T} + \frac{T_{\rm A}}{(T - T_{\rm V})^2} \right)^{-1/2} = {T_{\rm G}}^{-1/2} (T_{\rm zg} - T) \quad . \tag{34}$$

Fig. 5 shows a plot of the growth rate data from Fig. 4 according to Eq.(34), setting $T_{\rm A}$ = 1458 K, $T_{\rm V}$ = 327 K (from Ferry [13], confirmed by Friedrich in a recent measurement[14]). The linear extrapolation suggested by the equation yields $T_{\rm zg}$ = 275 °C . Prerequisite for an application of this procedure is a high accuracy of the measured growth rates so that the

derivative $\mathrm{d}\ln(u/u_0)/\mathrm{d}T$ can be reliably determined. Here this aim was obviously achieved. The error limits for T_{zg} remain below ± 2 °C . The continuous line in Fig.4 is a least squares data fit based on Eq.(4), leading to the same results for the adjusted parameters T_{zg} and T_{G}. Inclusion of the weak linear temperature dependence of u_0 according to Eq.(31) does not change the result.

Fig. 6 presents the (T, d^{-1}) nanophase diagram of iPS. The SAXS measurements yielded the crystallization and the recrystallization line, both ending at $T^{\infty}_{\mathrm{mc}} = 310$ °C . The location of the triple point $\mathrm{X_s}$ and the melting line followed from the series of DSC scans reproduced in Fig. 7. For crystallization temperatures up to 220 °C the final melting always takes place at 230 °C , which therefore represents the triple point temperature. The weak low temperature endotherms in the DSC diagrams are to be associated with the melting of some initial crystallites which do not participate in the recrystallization. Their locations established the melting line which ends at $T^{\infty}_{\mathrm{ac}} = 289$ °C [12]. With the knowledge of $T^{\infty}_{\mathrm{am}} = T_{\mathrm{zg}}$ from the growth rate measurement the a-m transition line is also exactly fixed: It starts from T^{∞}_{am} and passes through $\mathrm{X_s}$. Its intersection with the crystallization line determines the second triple point, $\mathrm{X_n}$. With this last step the nanophase diagram controlling crystallization and melting of iPS in bulk is complete. Table 2 gives the slope $-\mathrm{d}d^{-1}/\mathrm{d}T$ of the a-m transition line:

$$C_{\mathrm{m}} = \frac{\Delta h_{\mathrm{ma}}}{2\sigma_{\mathrm{am}} T^{\infty}_{\mathrm{am}} \Delta z} \quad , \tag{35}$$

of the melting line:

$$C_{\mathrm{f}} = \frac{\Delta h_{\mathrm{ca}}}{2\sigma_{\mathrm{ac_s}} T^{\infty}_{\mathrm{ac}} \Delta z} \quad , \tag{36}$$

of the crystallization line:

$$C_{\mathrm{c}} = \frac{\Delta s_{\mathrm{cm}}}{(2\sigma_{\mathrm{ac_n}} - 2\sigma_{\mathrm{am}})\Delta z} \quad , \tag{37}$$

and of the recrystallization line:

$$C_{\mathrm{r}} = \frac{\Delta s_{\mathrm{cm}}}{(2\sigma_{\mathrm{ac_s}} - 2\sigma_{\mathrm{am}})\Delta z} \quad . \tag{38}$$

It furthermore includes the macroscopic transition temperatures $T^{\infty}_{\rm am}, T^{\infty}_{\rm ac}, T^{\infty}_{\rm mc}$ and the growth activation temperature $T_{\rm G}$

Table 1: iPS: Data taken from Fig.5 and the nanophase diagram Fig.6

$T^{\infty}_{\rm am}$ °C	$T^{\infty}_{\rm ac}$ °C	$T^{\infty}_{\rm mc}$ °C	$C_{\rm m}$ $\rm nm^{-1}K^{-1}$	$C_{\rm f}$ $\rm nm^{-1}K^{-1}$	$C_{\rm c}$ $\rm nm^{-1}K^{-1}$	$C_{\rm r}$ $\rm nm^{-1}K^{-1}$	$T_{\rm G}$ K
275	289	310	3.66×10^{-3}	2.75×10^{-3}	1.66×10^{-3}	2.01×10^{-3}	788

Figs. 8 through 11 and table 2 present the analogous results for poly(ϵ-caprolactone). Optical measurements of spherulite growth rates - again down to minimum values of the order of a nanometer per minute - here were carried out in the temperature range between 48 °C and 58 °C , and the results are reproduced in Fig. 8. The linear extrapolation in Fig. 9 yields a zero growth temperature at 77 °C . The time- and temperature dependent SAXS experiments led to the crystallization-, recrystallization- and melting line included in the nanophase diagram of Fig. 10. The location of the triple point $X_{\rm s}$ is confirmed by the DSC scans shown in Fig. 11, which shows a constant melting temperature (57 °C) for all crystallization processes carried out below and at 40 °C . Knowledge of $T^{\infty}_{\rm am} = T_{\rm zg}$ allows to fix the a-m transition line and thus to complete the diagram. Table 2 collects all the data - macroscopic transition temperature and slopes of the transition lines - and gives also the value of $T_{\rm G}$ taken from Fig. 9.

Determination of the same properties of polyethylene is not as straightforward as for iPS and PϵCL, and it leaves questions open. Well determined are the zero growth temperature and the growth activation temperature. Both, the least squares fit through the growth rate data in Fig. 12 and the line through the data of Fig. 13 give $T_{\rm zg} = 132.5$ °C and $T_{\rm G} = 18$ K. Determination of the various transition lines in the nanophase diagram is hindered in linear polyethylenes by the crystal thickening in the solid state. For the crystallization- and

Table 2: PϵCL: Data taken from Fig.9 and the nanophase diagram Fig.10

T_{am}^{∞} °C	T_{ac}^{∞} °C	T_{mc}^{∞} °C	C_{m} $\mathrm{nm}^{-1}\mathrm{K}^{-1}$	C_{f} $\mathrm{nm}^{-1}\mathrm{K}^{-1}$	C_{c} $\mathrm{nm}^{-1}\mathrm{K}^{-1}$	C_{r} $\mathrm{nm}^{-1}\mathrm{K}^{-1}$	T_{G} K
77	99	135	6.90×10^{-3}	3.33×10^{-3}	1.54×10^{-3}	1.82×10^{-3}	397

the recrystallization line there is a way to overcome this problem: Since both remain unaffected by the presence of co-units, and co-units suppress the crystal thickening, these two transition lines can be taken over from the SAXS studies of poly(ethylene-co-octenes) and poly(ethylene-co-butenes) [11][15]. Fig. 14 includes these two lines, which both extrapolate to $T_{\mathrm{mc}}^{\infty} = 154$ °C . The nanophase diagram of linear polyethylene cannot be reliably determined because of the poorly known melting line. Since long time the dispute about the equilibrium melting point of polyethylene goes on, so far without conclusion. An extrapolation of n-alkane melting data on theoretical grounds led Flory and Vrij to $T_{\mathrm{ac}}^{\infty} = 144.7$ °C [16], whereas Wunderlich proposes on the basis of melting point determinations for large chain extended crystals $T_{\mathrm{ac}}^{\infty} = 141.4$ °C [17]. Our own investigations by SAXS on octene- and butene-copolymers did not allow a decision. Extrapolation of equilibrium melting points of copolymers to zero copolymer content yielded for one series 144 °C [11] and for the other series 141 °C [15], which just indicates the error limits of such extrapolations. We have included now in Fig. 14 the extrapolated melting line given in [11]. From this choice there follows the shown location of the triple point $\mathrm{X_s}$ and the shown a-m transition line which runs through $\mathrm{X_s}$ after a start at $T_{\mathrm{am}}^{\infty} = T_{\mathrm{zg}}$. Table 3 collects the data thus obtained for macroscopic transition temperatures and transition line slopes, setting the uncertain parameters in brackets.

Table 3: PE: Data taken from Fig.13 and the nanophase diagram Fig.14

T_{am}^{∞}	T_{ac}^{∞}	T_{mc}^{∞}	C_{m}	C_{f}	C_{c}	C_{r}	T_{G}
°C	°C	°C	$\mathrm{nm}^{-1}\mathrm{K}^{-1}$	$\mathrm{nm}^{-1}\mathrm{K}^{-1}$	$\mathrm{nm}^{-1}\mathrm{K}^{-1}$	$\mathrm{nm}^{-1}\mathrm{K}^{-1}$	K
132.5	(144)	154	(23.3×10^{-3})	(5.88×10^{-3})	3.12×10^{-3}	3.64×10^{-3}	18

5 Discussion

Evaluation of the experimental results collected in the previous section yields for each of the investigated systems

- the enthalpy change Δh_{ma} between the mesomorphic and the amorphous phase
- the surface free energy of mesomorphic lamellae σ_{am}
- the surface free energy of crystalline lamellae in the initial native state, $\sigma_{\mathrm{ac_n}}$
- the surface free energy of crystalline lamellae in the final stabilized state, $\sigma_{\mathrm{ac_s}}$
- the free energy barrier per monomer of the activation step Δf^{con}

Taking the heat of fusion, Δh_{ca}, from the literature, the heat of transition Δh_{ma} follows from an application of Eq.(7). In the next step σ_{am} is calculated using Eq.(35). The surface free energy $\sigma_{\mathrm{ac_n}}$ is obtained using Eq.(37) with Δs_{cm} defined by Eq.(11). The surface free energy of the stabilized crystallites can either be calculated applying the corresponding relation Eq.(38) or using Eq.(36). Finally, Δf^{con} is obtained by use of Eq.(32).

Table 4 refers to the experiments on i-polystyrene and contains all the thus obtained thermodynamic and kinetical parameters. The heat of transition Δh_{ma} is indicative for a truly intermediate character of the mesomorphic phase, being neither near to the liquid nor resembling a perturbed crystallite. Comparing mesomorphic with crystalline lamellae, the drop of

Table 4: iPS: Heats of transition, surface free energies and activation barrier as derived from the data in Table 1 ($\Delta z = 0.22$ nm, $\Delta h_{\rm ca}$ from [12])

$\Delta h_{\rm ma}$ $\frac{\rm kJ}{\rm mol\ C_8H_8}$	$\Delta h_{\rm ca}$ $\frac{\rm kJ}{\rm mol\ C_8H_8}$	$\sigma_{\rm am}$ $\frac{\rm kJ}{\rm mol}$	$\sigma_{\rm ac_n}$ $\frac{\rm kJ}{\rm mol}$	$\sigma_{\rm ac_s}$ $\frac{\rm kJ}{\rm mol}$	$\Delta f^{\rm con}$ $\frac{\rm kJ}{\rm mol\ C_8H_8}$
5.4	9.3	6.1	15.8	13.7	2.9

the surface free energy, from $\sigma_{\rm ac_n}$ and $\sigma_{\rm ac_s}$ to $\sigma_{\rm am}$, is larger than that in the heats of transition from $\Delta h_{\rm ca}$ to $\Delta h_{\rm ma}$. This is, indeed, an expected result. Only under this condition stabilities of crystalline and mesomorphic lamellae become inverted for nanocrystallites, thus opening the mesophase mediated growth route.

The value found for the free energy of activation, $\Delta f^{\rm con} = 2.9$ kJ per mole monomers, amounts to about half of the heat of transition $\Delta h_{\rm ma}$. This is a reasonable result when we associate the activation barrier with the chain straightening prior to an attachment. At $T^{\infty}_{\rm am}$ we have at equilibrium

$$0 = \Delta g_{\rm ma} = \Delta h_{\rm ma} - T\Delta s_{\rm ma} \quad . \tag{39}$$

Rather than decomposing $\Delta g_{\rm ma}$ into the total changes of enthalpy and entropy, $\Delta g_{\rm ma}$ can also be split up into an intermolecular and an intramolecular part, as

$$0 = \Delta g_{\rm ma} = \Delta h^{\rm int} - \Delta f^{\rm con} \quad . \tag{40}$$

Here $-\Delta f^{\rm con} < 0$ represents the drop in the conformational free energy accompanying the transition from the mesophase to the melt, and $\Delta h^{\rm int} > 0$ expresses the simultaneously weakened attractive van der Waals interchain interaction energy. Since $\Delta h_{\rm ma}$ includes both, $\Delta h^{\rm int}$ and the energy increase of coiled compared to straightened chains, we have

$$\Delta h_{\rm ma} > \Delta h^{\rm int} = \Delta f^{\rm con} \tag{41}$$

which basically agrees with the observation.

Table 5 shows the analogous set of data for poly(ϵ-caprolactone). Overall we find similar

Table 5: PϵCL: Heats of transition, surface free energies and activation barrier as derived from the data in Table 2 ($\Delta z = 0.85$ nm, $\Delta h_{\rm ca}$ from [11])

$\Delta h_{\rm ma}$ $\frac{\rm kJ}{\rm mol\ C_6H_{10}O_2}$	$\Delta h_{\rm ca}$ $\frac{\rm kJ}{\rm mol\ C_6H_{10}O_2}$	$\sigma_{\rm am}$ $\frac{\rm kJ}{\rm mol}$	$\sigma_{\rm ac_n}$ $\frac{\rm kJ}{\rm mol}$	$\sigma_{\rm ac_s}$ $\frac{\rm kJ}{\rm mol}$	$\Delta f^{\rm con}$ $\frac{\rm kJ}{\rm mol\ C_6H_{10}O_2}$
10.5	17.9	2.5	9.9	8.5	6.86

properties as for iPS

- $\Delta h_{\rm ma}$ suggests a mesophase character intermediate between the melt and the crystallites,
- the preference for the mesophase in thin lamellae is due to the much lower surface free energy
- the stabilization of the initial native crystals is caused by a drop of the surface free energy ($\sigma_{\rm ac_n} > \sigma_{\rm ac_s}$)
- the activation free energy corresponds to a large part of the heat of transition $\Delta h_{\rm ma}$.

Looking more closely, one notes remarkable differences in two of the experimental parameters, namely in $C_{\rm m}$ and $T_{\rm G}$. $C_{\rm m}$ measures the strength of surface effects in mesomorphic lamellae. According to Eq.(35) effects are weaker for higher values of $C_{\rm m}$, hence, much weaker in PϵCL when compared to iPS. The growth activation temperature $T_{\rm G}$ decides upon the rise of growth rates with decreasing temperature. For rapidly crystallizing systems $T_{\rm G}$ is low, for slowly crystallizing systems $T_{\rm G}$ is high. The much higher value of $T_{\rm G}$ for iPS compared to PϵCL just expresses this behavior. Looking at Eq.(32) we find two different factors of influence

- Crystallization is accelerated if the activation barrier Δf^{con}, or better, the barrier per unit chain length, referred to the thermal energy,

$$\frac{\Delta f^{\mathrm{con}}}{RT^{\infty}_{\mathrm{am}}\Delta z} \quad ,$$

  is low.

- Crystallization is accelerated if C_{m} is high, i.e., the surface free energy of mesomorphic layers has a low value.

So, what is the reason for the more rapid crystallization of PϵCL compared to iPS? The value of the two factors of influence are

for iPS: $\Delta f^{\mathrm{con}}/(RT^{\infty}_{\mathrm{am}}\Delta z) = 2.89\ \mathrm{nm}^{-1}$, $C_{\mathrm{m}} = 3.66 \times 10^{-3}\ \mathrm{nm}^{-1}\ \mathrm{K}^{-1}$

for PϵCL: $\Delta f^{\mathrm{con}}/(RT^{\infty}_{\mathrm{am}}\Delta z) = 2.74\ \mathrm{nm}^{-1}$, $C_{\mathrm{m}} = 6.90 \times 10^{-3}\ \mathrm{nm}^{-1}\ \mathrm{K}^{-1}$.

This means: The only reason is the much lower surface free energy of the mesomorphic lamellae of PϵCL only. The kinetical factor, which controls the dynamics at the growth face has practically equal values for both systems. Interesting to note, the thickness of the crystal lamella changes in iPS and PϵCL with temperature in comparable manner, as is indicated by the similar values of C_{c}. The difference lies in the entrance step: The initial thickness of the mesomorphic layers at a certain supercooling below T^{∞}_{am} is for PϵCL much smaller than for iPS. This facilitates the chain attachment and leads to a higher growth rate.

As mentioned previously, the experimental data for linear polyethylene are partly accurate, and partly uncertain. If we apply the same evaluation procedures as for iPS and PϵCL we obtain for the thermodynamic parameters and the kinetical factor Δf^{con} the values given in Table 6. Some of the quantities are useful, having acceptable error limits. This holds for the heat of transition Δh_{ma} and the surface free energies $\sigma_{\mathrm{ac_n}}$ and $\sigma_{\mathrm{ac_s}}$ of native and stabilized crystals. Δh_{ma} would become 20% larger, if T^{∞}_{ac} is set to 141 °C , and a similar error range exists for the surface free energies. However, this does not affect the main conclusion: The

Table 6: PE: Heats of transition, surface free energies and activation barrier as derived from the data in Table 3 ($\Delta z = 0.25$ nm, $\Delta h_{\rm ca}$ from [11])

$\Delta h_{\rm ma}$ $\frac{\rm kJ}{\rm mol\ C_2H_4}$	$\Delta h_{\rm ca}$ $\frac{\rm kJ}{\rm mol\ C_2H_4}$	$\sigma_{\rm am}$ $\frac{\rm kJ}{\rm mol}$	$\sigma_{\rm ac_n}$ $\frac{\rm kJ}{\rm mol}$	$\sigma_{\rm ac_s}$ $\frac{\rm kJ}{\rm mol}$	$\Delta f^{\rm con}$ $\frac{\rm kJ}{\rm mol\ C_2H_4}$
3.7	8.2	0.82	7.7	6.7	0.35

mesomorphic phase of PE has again an intermediate character, being neither solid nor melt like. Indeed, arguments have been presented in support of an identity with the hexagonal phase which becomes macroscopically stable at high pressures and temperatures [7].

Absolutely uncertain are the values for $\sigma_{\rm am}$ and $\Delta f^{\rm con}$, because they are extremely sensitive with regard to the choice of the triple point $X_{\rm s}$. A slight variation of the melting line shifts $X_{\rm s}$ in a way that the a-m transition line changes its slope, $C_{\rm m}$, drastically. The result are correspondingly large changes in $\sigma_{\rm am}$ and $\Delta f^{\rm con}$. In fact, when comparing $\Delta f^{\rm con}$ with $\Delta h_{\rm ma}$ or a theoretical estimate, doubts arise. For iPS and PϵCL, $\Delta f^{\rm con}$ amounts to more than half of $\Delta h_{\rm ma}$, which is reasonable; now we have a value one order of magnitude below $\Delta h_{\rm am}$, which appears improbable. A calculation of the change of the conformational free energy resulting from a transition from the all-trans to the coiled state of PE in the framework of Flory's RIS model yields 4.5 kJ/mol C_2H_4[18]. The difference $\Delta f^{\rm con}$ between the coiled state and the mesophase is of course smaller, but not by one order of magnitude. One therefore might think that the triple point is located at a slightly higher temperature, and that $\Delta f^{\rm con}$ as well as $C_{\rm m}$ are larger than the values given in Tables 3 and 6. The peculiar result in the experimental data of PE is the extremely low value of $T_{\rm G}$, which is the expression for the easiness of crystallization in PE. Is it due to a particularly low activation barrier or a particularly low surface free energy of mesomorphic PE layers ? We cannot give a definite answer, but since the surface free energy

σ_{am} is for sure much lower than in the other systems it is most probably the main responsible for the rapid crystallization of PE.

With the a-m transition line also the triple point $\mathrm{X_n}$ is fixed for each system, being located at the intersection with the crystallization line. The point $\mathrm{X_n}$, being shown in all three nanophase diagrams, marks the respective end of the mesophase-mediated growth process. For crystallization temperatures above $T(\mathrm{X_n})$ and crystal thicknesses above $d(\mathrm{X_n})$ growth must proceed by a direct attachment of chain sequences onto the lateral growth face of the crystal. As it appears, so far experiments never entered this temperature range. In principle, polymers also crystallize between $T(\mathrm{X_n})$ and T_{ac}^{∞}, however, as it seems, this occurs with a vanishingly low rate. For the observed, acceptable crystallization rates the participation of an intermediate mesomorphic phase is obviously a necessity.

Acknowledgements

Support of this work by the Deutsche Forschungsgemeinschaft is gratefully acknowledged. Thanks are also due to the Fonds der Chemischen Industrie for financial help.

References

[1] J.D Hoffman, G.T Davis, and J.I. Lauritzen. In *Treatise on Solid State Chemistry* Vol.3, N.B.Hannay Ed., page 497. Plenum, 1976.

[2] P.J. Barham, R.A. Chivers, A. Keller, J. Martinez-Salazar, and S.J. Organ. *J.Mater.Sci.*, 20:1625, 1985.

[3] G. Strobl. *Progr.Polym.Sci.*, 31:398, 2006.

[4] T.Y. Cho, W. Stille, and G. Strobl. *Colloid Polym Sci*, in press, 2007.

[5] T.Y. Cho, W. Stille, and G. Strobl. *Macromolecules*, 40, 2007.

[6] G. Strobl. *Eur.Phys.J.E*, 3:165, 2000.

[7] G. Strobl. *Eur.Phys.J.E*, 18:295, 2005.

[8] T.Y. Cho, B. Heck, and G. Strobl. *Chinese J.Polym.Sci.*, 25:83, 2007.

[9] T. Hippler, S. Jiang, and G. Strobl. *Macromolecules*, 38:9396, 2005.

[10] B. Heck, S. Siegenführ, G. Strobl, and R. Thomann. *Polymer*, 48:1352, 2007.

[11] B. Heck, T. Hugel, M. Iijima, E. Sadiku, and G. Strobl. *New J.Physics*, 1:17, 1999.

[12] M. Al-Hussein and G. Strobl. *Macromolecules*, 35:8515, 2002.

[13] J.D. Ferry, W.C. Child, R. Zand, D.M. Stern, M.L. Williams, and R.F. Landel. *J.Colloid Sci.*, 12:53, 1957.

[14] C. Friedrich. *private communication*, 2006.

[15] T.Y. Cho, B. Heck, and G. Strobl. *Colloid Polym.Sci.*, 282:825, 2004.

[16] P.J. Flory and A. Vrij. *J.Am.Chem.Soc.*, 85:3548, 1963.

[17] B. Wunderlich. *Macromolecular Physics, Volume 3*, page 58. Academic Press, 1980.

[18] G. Strobl. *The Physics of Polymers. 3rd Edition*, page 64. Springer, 2007.

[19] S. Acierno, E. Di Maio, S. Iannace, and N. Grizzuti. *Rheol.Acta*, 45:387, 2006.

[20] J.P. Armistead and J.D. Hoffman. *Macromolecules*, 35:3895, 2002.

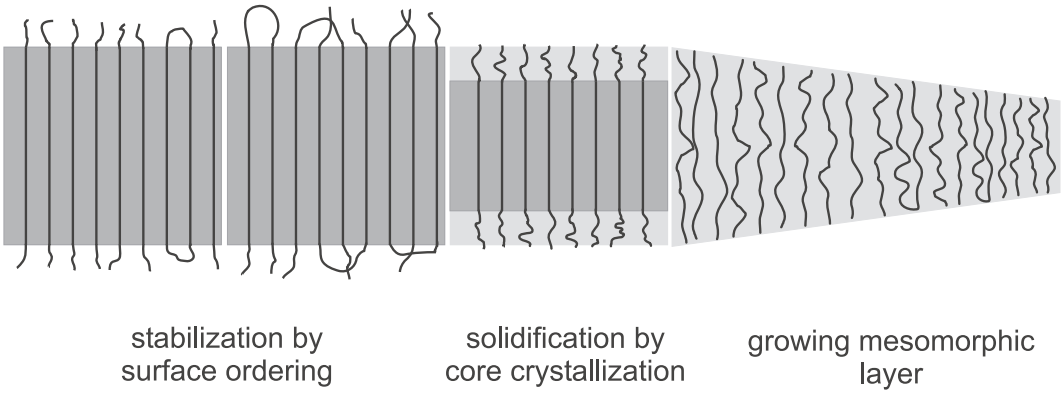

Figure 1: Multistage model: Pathway followed in the growth of polymer crystallites

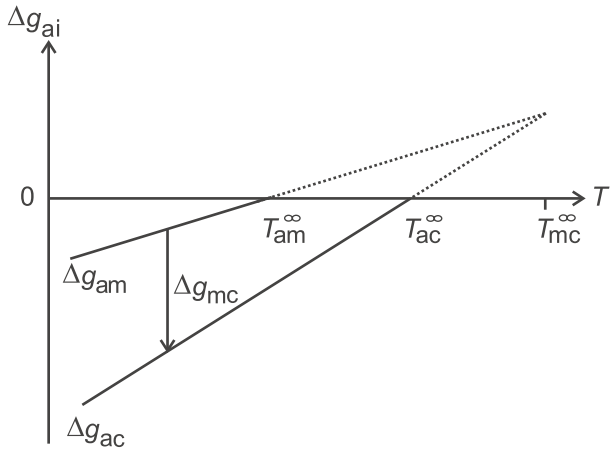

Figure 2: Thermodynamic conditions assumed for crystallizing polymers: Temperature dependence of the chemical potentials of a mesomorphic and the crystalline phase. The potentials are referred to the chemical potential of the melt and denoted $\Delta g_{\rm am}$ and $\Delta g_{\rm ac}$

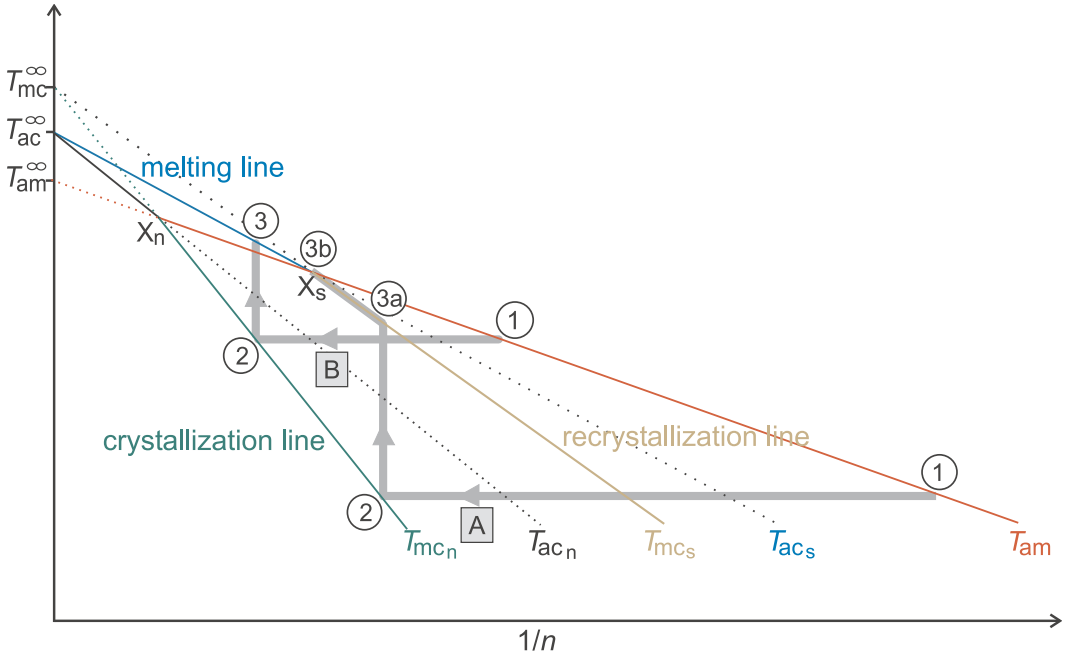

Figure 3: (T/n^{-1}) nanophase diagram for polymer layers in a melt (label a) dealing with three phases: mesomorphic (m), native crystalline (c_n) and stabilized crystalline (c_s). Lines of size dependent phase transitions: crystallization line T_{mc_n}, recrystallization line T_{mc_s}, melting line T_{ac_s}, a-m transition line T_{am}. Two routes for an isothermal crystallization followed by heating; A (low crystallization temperatures) and B (high crystallization temperatures)(from [7])

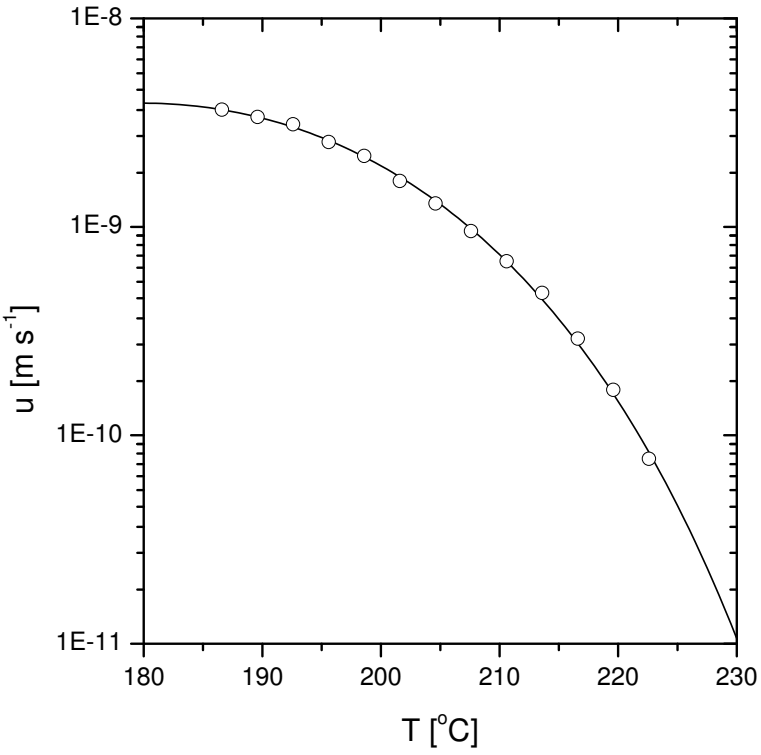

Figure 4: iPS: Temperature dependence of the radial growth rate. The adjusted curve corresponds to Eq. (4) with $T_{\mathrm{A}} = 1458$ K, T_{V}=327K [13], T_{G}=788 K and $T_{\mathrm{zg}} = 275$ °C

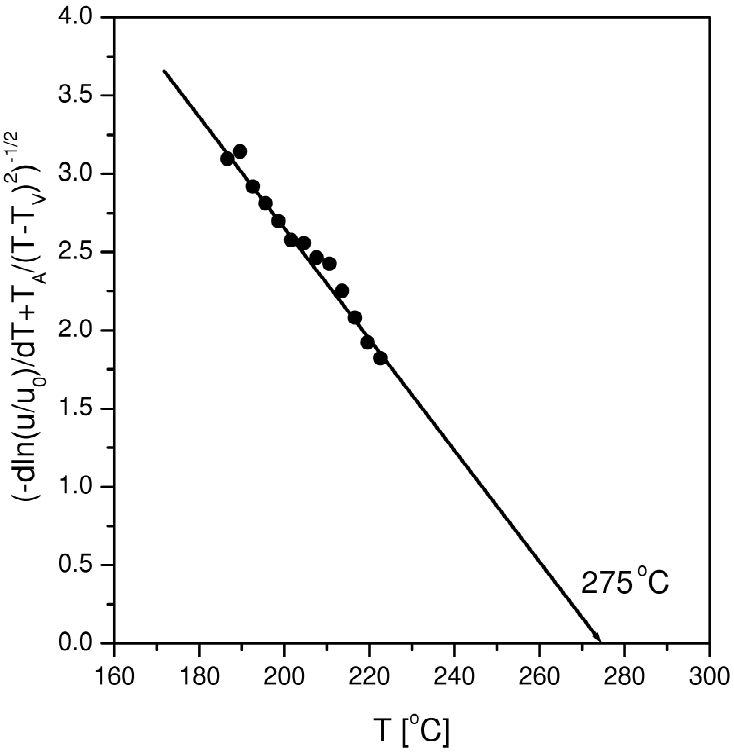

Figure 5: iPS: Plot based on Eq.(34) giving $T_{zg} = 275$ °C

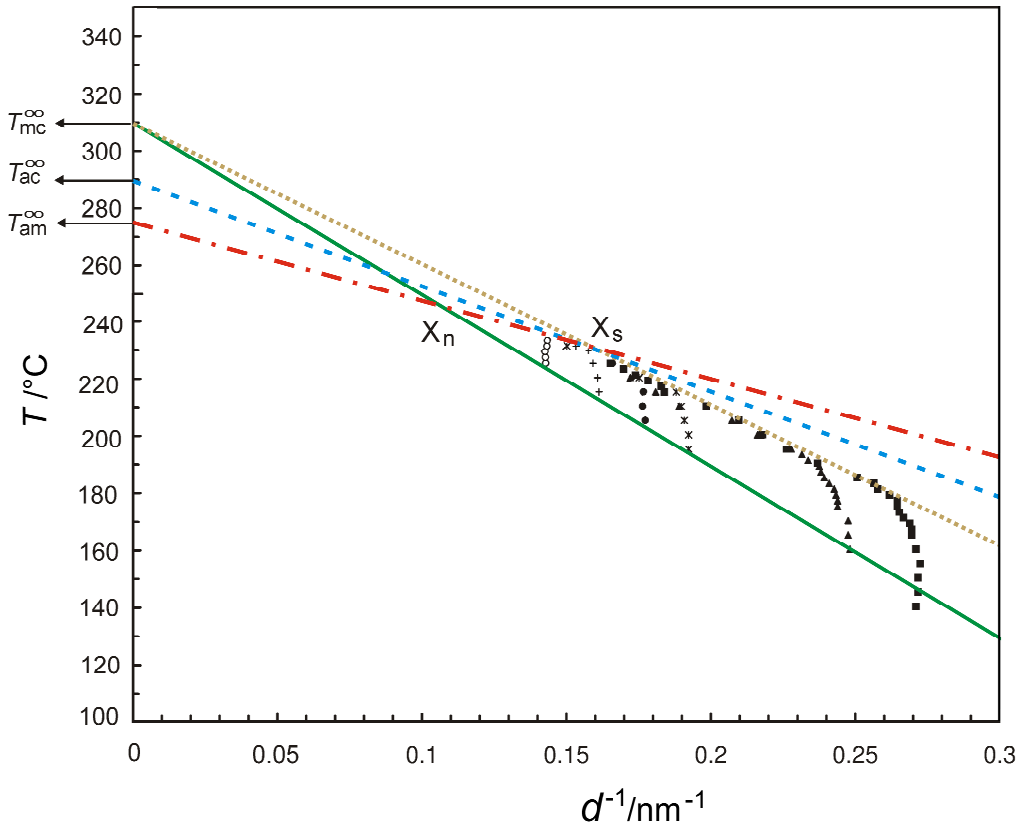

Figure 6: iPS: Crystallization line, recrystallization line (*dots*) and melting line (*dashes*) determined by SAXS and DSC[12], zero growth temperature T_{am}^{∞} from Fig.5 and a-m transition line (*dash-dots*)

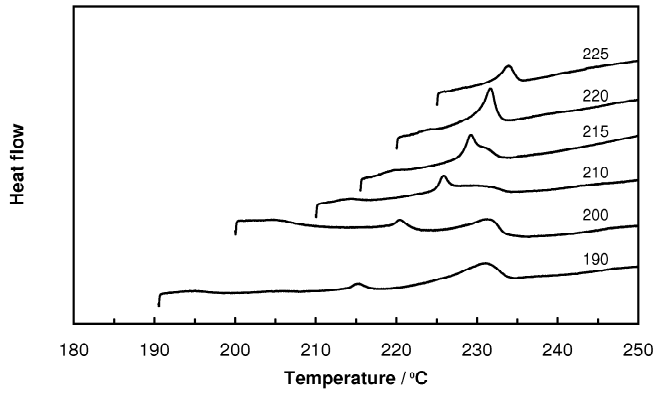

Figure 7: iPS: DSC melting curves obtained after crystallizations at various temperatures between 180 °C and 225 °C , indicating a triple point temperature $T(\mathrm{X_s})$ ≈230 °C [12]

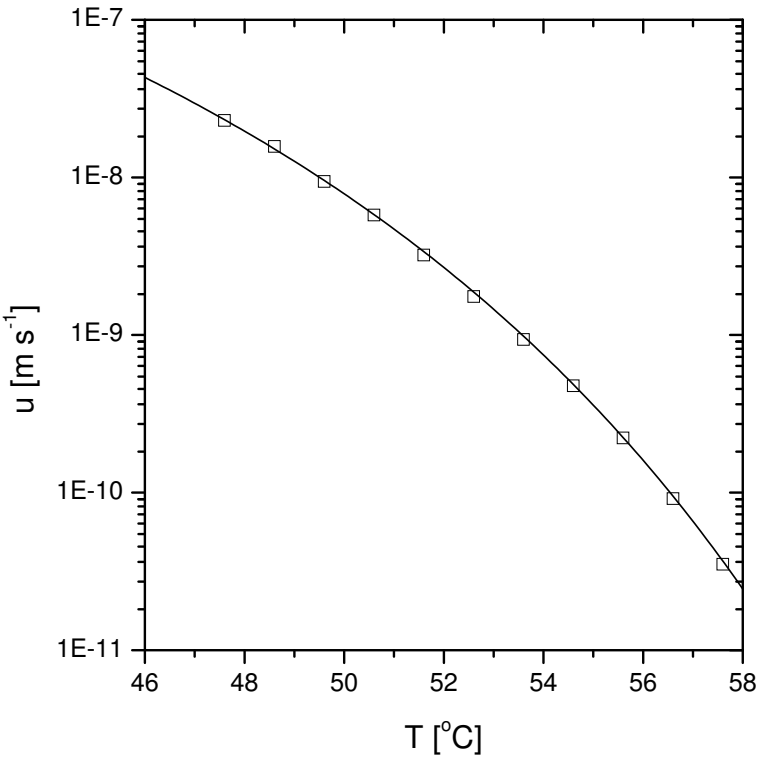

Figure 8: PϵCL: Temperature dependence of the radial growth rate. Representation by Eq. (4) with $T_\mathrm{A} = 4650$ K ($T_\mathrm{V} = 0$)[19], T_G=397 K and $T_\mathrm{zg} = 77$ °C (from [4])

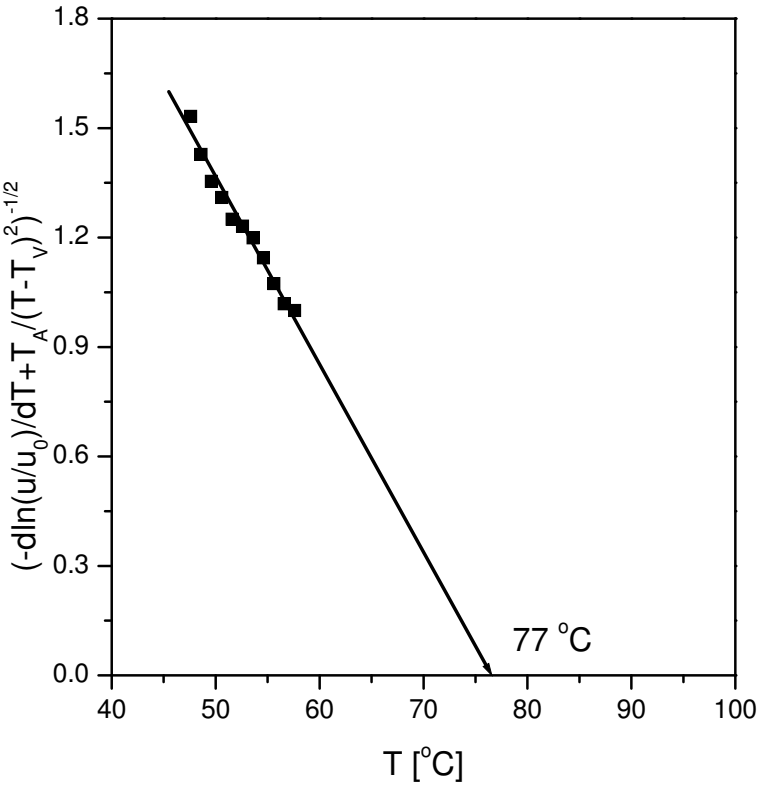

Figure 9: PϵCL: Plot based on Eq.(34) giving $T_{\rm zg} = 77$ °C (from [4])

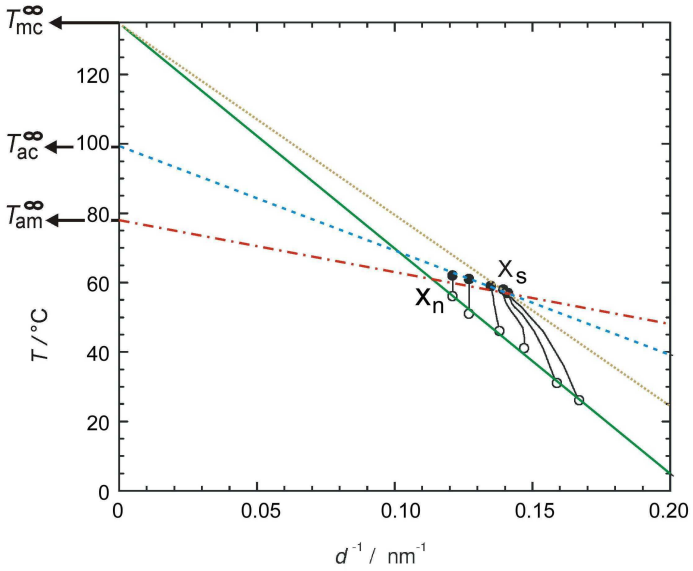

Figure 10: PϵCL: Crystallization line, recrystallization line (*dots*) and melting line (*dashes*) determined by SAXS[11], zero growth temperature $T_{\rm am}^{\infty}$ from Fig.9 and a-m transition line (*dash-dots*). The solid lines connecting the beginning and the end of each heating process show the experimentally determined crystal thickness variations

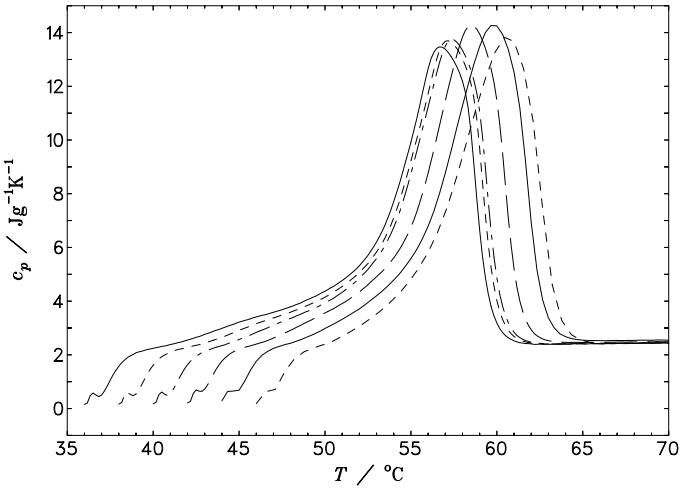

Figure 11: PϵCL: DSC melting curves obtained after crystallizations at various temperatures between 37 °C and 47 °C (heating rate 10 K/min), indicating a triple point temperature $T(\mathrm{X_s})$=57 °C [11]

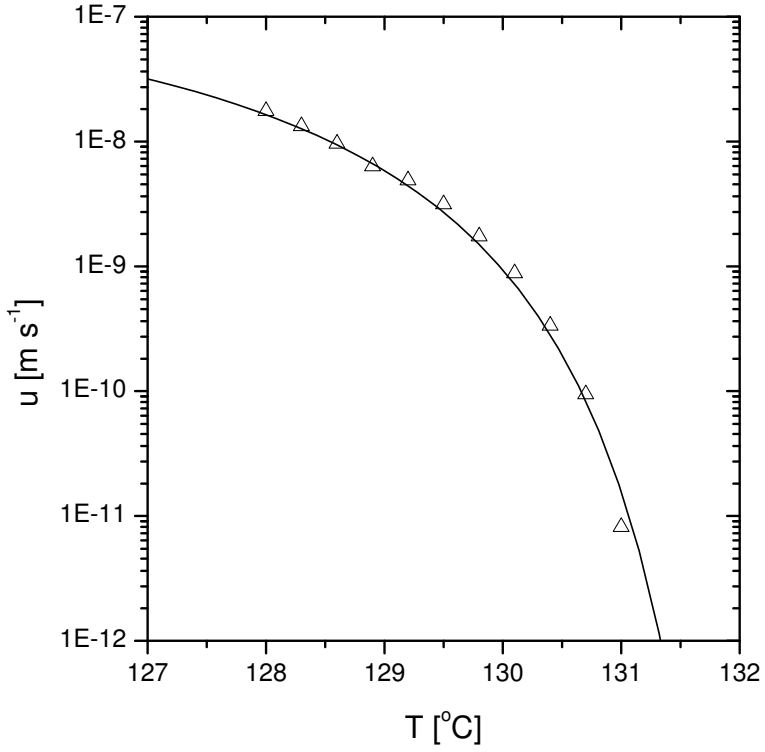

Figure 12: Linear PE (M_w = 6×10^4 g mol^{-1}): Temperature dependence of the radial growth rate. Data representation based on Eq.(8) with T_A=2890 K (T_V=0K)[20], T_G=18 K, T_{zg} = 132.5 °C (from [5])

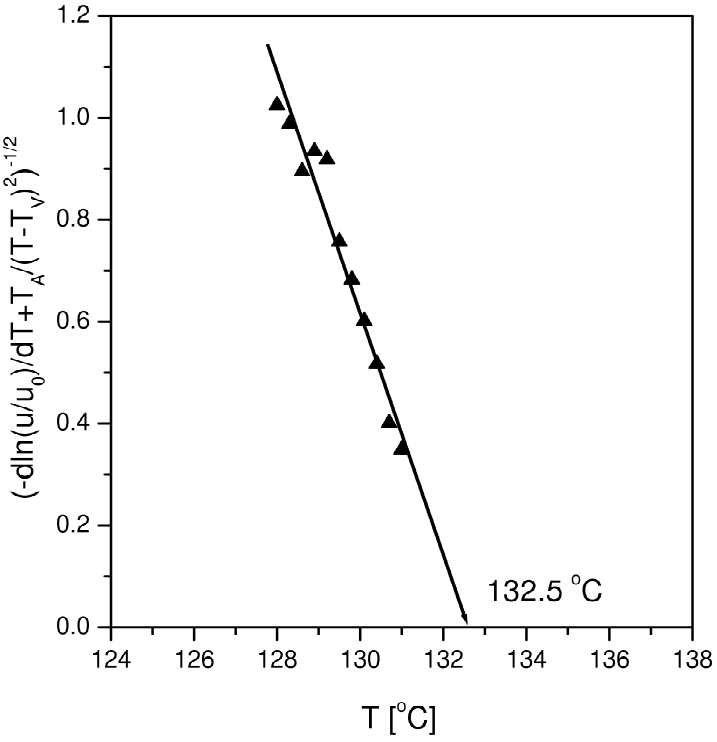

Figure 13: Linear PE: Data from Fig.12 represented according to Eq.(34). The result for T_{zg} is 132.5 °C (from [5])

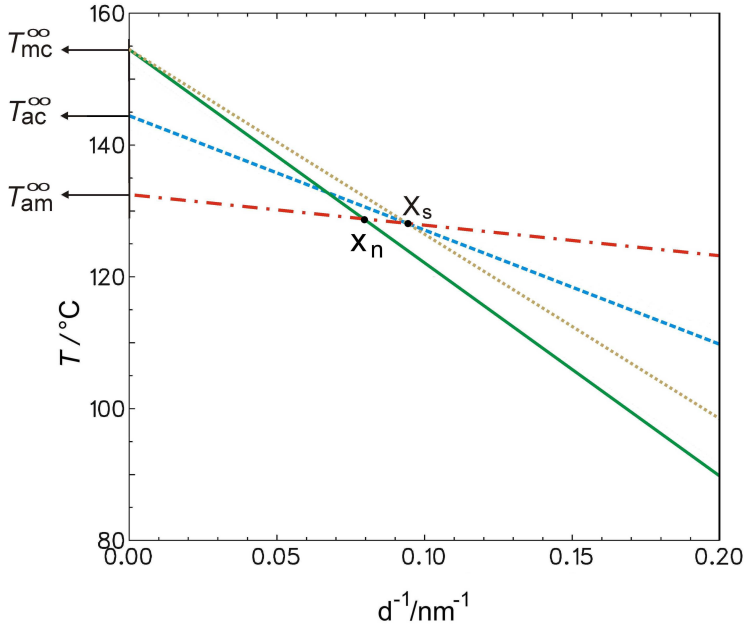

Figure 14: Linear PE: Crystallization line, recrystallization line (*dots*) and melting line (*dashes*) determined by SAXS[11][7], zero growth temperature $T_{\rm am}^{\infty}$ from Fig.13 and a-m transition line (*dash-dots*)